

---

# Enhancing Score-Based Sampling Methods with Ensembles

---

Tobias Bischoff<sup>\*1</sup> Bryan Riel<sup>\*2</sup>

## Abstract

We introduce ensembles within score-based sampling methods to develop gradient-free approximate sampling techniques that leverage the collective dynamics of particle ensembles to compute approximate reverse diffusion drifts. We introduce the underlying methodology, emphasizing its relationship with generative diffusion models and the previously introduced Föllmer sampler. We demonstrate the efficacy of ensemble strategies through various examples, ranging from low- to medium-dimensionality sampling problems, including multi-modal and highly non-Gaussian probability distributions, and provide comparisons to traditional methods like NUTS. Our findings highlight the potential of ensemble strategies for modeling complex probability distributions in situations where gradients are unavailable. Finally, we showcase its application in the context of Bayesian inversion problems within the geophysical sciences.

## 1. Introduction

Gradient-free methods for sampling from probability distributions are crucial in scenarios where gradient information is unavailable or computationally prohibitive. Unfortunately, many performant samplers such as the No U-Turn Sampler (NUTS) or the Metropolis Adjusted Langevin Algorithm (MALA) require gradient information to fully realize their advantages (Roberts & Tweedie, 1996; Hoffman et al., 2014). Others have investigated the use of transport based sampling methods to generate samples from probability distributions through stochastic differential equations, e.g., Huang et al. (2021); Vargas et al. (2023). In this context, Huang et al. (2021) have suggested a Monte Carlo approximation of the Föllmer drift to sample from probability distributions (Föllmer, 1985; 1986). They show that

this approach results in an approximation to the solution of the Schrödinger bridge problem (Schrödinger, 1932). We build on these ideas and introduce ensemble strategies that leverage the collective dynamics of a particle ensemble to approximately compute the score function within a reverse diffusion process. Compared to the aforementioned Föllmer sampler, a goal is to reduce evaluations of the probability distribution that one wants to sample from. In the setting of Bayesian inverse problems, this helps to reduce forward model evaluations, thereby offering an efficient sampling technique. More concretely, we introduce an importance sampling Monte Carlo estimator for the score function of a forward diffusion process in order to sample from a probability distribution using the associated reverse diffusion process. Because there is some flexibility in the choice of forward diffusion process, we can design samplers that are still useful at medium- to high-dimensionality.

This work details the foundational methodology of our ensemble strategies, emphasizing its connection with generative diffusion models and the pre-existing Föllmer sampler. We assess the performance of our method through a range of diverse examples, encompassing low- to medium-dimensional Bayesian inference problems, including multi-modal and non-elliptical distributions. Our comparative analysis with Markov Chain Monte Carlo (MCMC) methods that utilize gradient information (e.g., Roberts & Tweedie, 1996; Hoffman et al., 2014) highlights the effectiveness of ensemble strategies in modeling complex probability distributions when gradients are not available. Furthermore, we demonstrate the practical application of our method in Bayesian inversion problems, particularly in the geophysical sciences where the dimensionality of the problem at hand can be of medium to large size, showcasing its potential for sophisticated probabilistic modeling.

### 1.1. Related Work

This paper builds upon existing research in stochastic processes, particularly focusing on the integration of Schrödinger-Föllmer approaches and particle and ensemble methods in computational physics (see, for example, Reich (2019) or Calvello et al. (2022) for recent overviews). Recent contributions adjacent to this area also include the work by Boffi & Vanden-Eijnden (2023) on the probability flow solution of the Fokker-Planck equation and the study

---

<sup>\*</sup>Equal contribution <sup>1</sup>Independent Researcher, Pasadena, CA, USA <sup>2</sup>School of Earth Sciences, Zhejiang University, Hangzhou, China. Correspondence to: Tobias Bischoff <bischtob@gmail.com>, Bryan Riel <briel@zju.edu.cn>.

by Bunne et al. (2022) on recovering stochastic dynamics through Gaussian Schrödinger bridges. Further, Dai et al. (2021) explored aspects of global optimization using Schrödinger-Föllmer diffusion. Huang et al. (2021) and Jiao et al. (2021) provided an initial analysis of the error and convergence properties of Schrödinger-Föllmer samplers in non-convex settings and introduced ideas this work was inspired by. Building on this, Zhang & Chen (2022) and Vargas et al. (2023) demonstrated the use of neural networks to improve the efficiency of Föllmer drift estimates in high-dimensional settings, and Bortoli et al. (2023) related the Schrödinger-Föllmer perspective to score-based generative models. In the area of ensemble-based gradient-free sampling techniques, Ensemble Kalman Inversion (EKI; e.g., Schillings & Stuart (2017)), Ensemble Kalman Sampling (EKS; Garbuno-Inigo et al. (2020)), and related variants have been developed to address situation where gradients are unavailable. See Chada (2022) or the aforementioned Calvello et al. (2022) for overviews.

## 1.2. Our Contributions

This work introduces ensemble strategies to calculate estimates of score functions. Our main contribution is an importance sampling Monte Carlo estimator that reuses the samples being generated in a reverse diffusion process to define an importance sampling distribution. This approach has the advantage of keeping the Monte Carlo samples necessary for estimating the score function of the reverse diffusion process low. Furthermore, we conduct extensive experiments with a hierarchy of problems, comparing our method against MCMC methods that utilize gradient information to improve sample efficiency (e.g., NUTS by Hoffman et al. (2014)). Lastly, we explore various parameters influencing performance, such as noise schedules, importance sampling strategies, and ensemble sizes, providing insights into its application in complex systems modeling. We also show how flexibility resulting from the choice of forward diffusion process can lead to performant algorithms that efficiently leverage prior information.

## 2. Theory

This section introduces the theoretical foundations for what follows, establishing the mathematical framework and principles that guide our methodology. We first give a quick overview of score-based sampling with diffusion models and then address some of the strategies that make our methods work for the demonstrated experiments.

### 2.1. Forward & Reverse Diffusion Processes

This section introduces the fundamental concepts of diffusion processes as they are used in this paper. Going forward, we consider forward diffusion processes of Ornstein-

Uhlenbeck form

$$d\mathbf{x} = -\mathbf{b}_t(\mathbf{x} - \boldsymbol{\mu}) dt + \mathbf{g}_t d\mathbf{W}_t, \quad (1)$$

where  $\mathbf{b}_t$  is a time-dependent linear operator,  $\boldsymbol{\mu}$  is the mean vector the process reverts to, and  $\mathbf{g}_t$  is a time-dependent scaling matrix (often referred to as the drift and diffusion operators, respectively). The associated reverse diffusion process (Anderson, 1982) is given by

$$d\mathbf{x} = -(\mathbf{b}_t(\mathbf{x} - \boldsymbol{\mu}) + \mathbf{g}_t \mathbf{g}_t^T \mathbf{s}_t(\mathbf{x})) dt + \mathbf{g}_t d\mathbf{W}_t, \quad (2)$$

where  $\mathbf{s}_t$  is the score of the solution of the forward diffusion equation and where Equation (2) is integrated backwards in time. This forward-reverse duality has been leveraged in numerous studies within the areas of generative machine learning to generate samples from high dimensional data distributions, e.g., Song & Ermon (2019); Song et al. (2021) and follow-on studies. For a given initial probability distribution  $p_0$  that we want to sample from, we can write down an exact expression for the score related to the process in Equation (1):

$$\mathbf{s}_t(\mathbf{x}) = \nabla \log p_t(\mathbf{x}) \quad (3a)$$

$$p_t(\mathbf{x}) = \int \kappa_t(\mathbf{x}|\mathbf{x}') p_0(\mathbf{x}') d\mathbf{x}' \quad (3b)$$

$$\kappa_t(\mathbf{x}|\mathbf{x}') = \mathcal{N}(\boldsymbol{\mu}_t(\mathbf{x}'), \boldsymbol{\Sigma}_t), \quad (3c)$$

where  $p_t$  is the solution to the Fokker-Planck equation associated with Equation (1) and the kernel function  $\kappa_t$  is a Gaussian corresponding to the associated Green's function. The kernel mean and covariance are given (Gardiner et al., 1985) as

$$\boldsymbol{\mu}_t(\mathbf{x}') = \left(1 - e^{-\int_0^t \mathbf{b}_{t'} dt'}\right) \boldsymbol{\mu} + e^{-\int_0^t \mathbf{b}_{t'} dt'} \mathbf{x}' \quad (4a)$$

$$\boldsymbol{\Sigma}_t = \int_0^t e^{-\int_{t'}^t \mathbf{b}_{t''} dt''} \mathbf{g}_{t'} \mathbf{g}_{t'}^T e^{-\int_{t'}^t \mathbf{b}_{t''} dt''} dt'. \quad (4b)$$

Having an analytic kernel is possible because the forward diffusion process is of Ornstein-Uhlenbeck form. We can see that the solution to the forward diffusion equation interpolates between the initial distribution  $p_0$  and a normal distribution as  $t \rightarrow \infty$ . In general, we choose  $\mathbf{b}_t$  in such a manner that at  $t = 1$  the forward diffusion has approximately converged to this normal distribution.

### 2.2. Bayesian Context

In a Bayesian context, when  $p_0$  is a posterior distribution, and if the prior distribution is a normal distribution with a given mean and covariance, then this approach can be used to approximately transport samples from the prior to the posterior over a time span  $[0, 1]$  by choosing  $\mathbf{b}_t$  and  $\mathbf{g}_t$  appropriately. Given the kernel of the forward diffusion process, one can use the reverse diffusion equation to draw

samples from  $p_0$ . However, the main challenge lies in the fact that the score  $\mathbf{s}_t$  is only available as a potentially high-dimensional integral. In the next sections, we introduce an approach that uses an ensemble of samples to define an importance sampling estimator for the score, thereby alleviating this problem for low- to medium-dimensional problems.

### 2.3. Estimating the Score Function

A key aspect of our ensemble strategies is the estimation of the score within the reverse diffusion process, which is essential for accurately simulating particle trajectories in Equation (2). This section outlines our approach to estimating the score function. To that end, we introduce an importance sampling distribution  $p_{\text{is}}$  (e.g., [Elvira & Martino, 2022](#)) such that we can rewrite the solution to the forward diffusion equation as

$$p_t(\mathbf{x}) = \int \kappa_t(\mathbf{x}|\mathbf{x}') \frac{p_0(\mathbf{x}')}{p_{\text{is}}(\mathbf{x}')} p_{\text{is}}(\mathbf{x}') d\mathbf{x}'. \quad (5)$$

We now proceed to define a Monte Carlo approximation of the form

$$\hat{p}_t(\mathbf{x}) = \frac{1}{N} \sum_{i=1}^N \kappa_t(\mathbf{x}|\mathbf{x}'_i) \frac{p_0(\mathbf{x}'_i)}{p_{\text{is}}(\mathbf{x}'_i)}, \quad \mathbf{x}'_i \sim p_{\text{is}}, \quad (6)$$

where  $N$  is the number of Monte Carlo samples drawn. Here, our goal is to define  $p_{\text{is}}$  in such a way that the reverse diffusion process generates good samples from the posterior distribution  $p_0$  even though we use an approximation for the score. When actually computing the estimate  $\hat{\mathbf{s}}_t(\mathbf{x}) = \nabla \log \hat{p}_t(\mathbf{x})$  for the score function, we follow the approach of [Vargas et al. \(2023\)](#) and use the logsumexp trick to dramatically improve the numerical stability of the score estimation. We further discuss several variance reduction strategies for the Monte Carlo estimator  $\hat{p}_t$  in the next section.

### 2.4. Variance Reduction Strategies

This section focuses on the implementation of various variance reduction strategies that are essential for enhancing the accuracy and efficiency of the sample generation process.

#### 2.4.1. IMPORTANCE SAMPLING VIA SAMPLE ENSEMBLE

One key aspect of our approach is to simultaneously consider ensembles of samples that are being generated. That is to say, we consider not just a single sample being generated in the reverse diffusion process, but rather an ensemble  $\{\mathbf{x}_i \in \mathbb{R}^D\}_{1 \dots N_{\text{ens}}}$ , where  $N_{\text{ens}}$  is the ensemble size. At  $t = 1$ , the initial conditions for the reverse diffusion process are drawn from a normal distribution. Then, as  $t$  is reduced from 1 to 0, the normal distribution samples are transformed

into samples from the distribution  $p_0$ . As the ensemble progresses, we can define an ensemble mean and covariance as

$$\boldsymbol{\mu}_{\text{ens}} = \frac{\sum_{i=1}^{N_{\text{ens}}} \mathbf{x}_i}{N_{\text{ens}}} \quad (7a)$$

$$\boldsymbol{\Sigma}_{\text{ens}} = \frac{\sum_{i=1}^{N_{\text{ens}}} (\mathbf{x}_i - \boldsymbol{\mu}_{\text{ens}})(\mathbf{x}_i - \boldsymbol{\mu}_{\text{ens}})^T}{N_{\text{ens}}} \quad (7b)$$

and an associated importance sampling distribution

$$p_{\text{is}} = \mathcal{N}(\boldsymbol{\mu}_{\text{ens}}, \boldsymbol{\Sigma}_{\text{ens}}). \quad (8)$$

Utilizing this ensemble-based  $p_{\text{is}}$  therefore relies on the adequacy of the normal distribution. In practice, we also set the number of Monte Carlo samples  $N$  equal to the ensemble size  $N_{\text{ens}}$ . We outline an alternative importance sampling distribution using a multiple importance sampling strategy based on the ensemble of samples in Appendix E. We find that both distributions work similarly well for the examples presented in this paper. The actual variance reduction achieved is directly related to the ensemble size; that is, as the ensemble size tends to infinity, the score estimator becomes exact. In practice, we find that we do not need to actually draw samples from  $p_{\text{is}}$  when calculating estimators for  $\hat{p}_t$  or  $\hat{\mathbf{s}}_t$ . Instead, we find that evaluating the Monte Carlo approximation at the ensemble members gives equally reasonable results.

#### 2.4.2. ANTITHETIC SAMPLING

We also find in our experiments that an antithetic sampling strategy can be beneficial to enhance the quality of the importance sampling estimator. The antithetic version of the importance sampling estimator can be written as

$$\hat{p}_t(\mathbf{x}) = \frac{\sum_{i=1}^{N_{\text{ens}}} \kappa_t(\mathbf{x}|\mathbf{x}'_i) \frac{p_0(\mathbf{x}'_i)}{p_{\text{is}}(\mathbf{x}'_i)}}{2N_{\text{ens}}} + \frac{\sum_{i=1}^{N_{\text{ens}}} \kappa_t(\mathbf{x}|-\mathbf{x}'_i) \frac{p_0(-\mathbf{x}'_i)}{p_{\text{is}}(-\mathbf{x}'_i)}}{2N_{\text{ens}}}. \quad (9)$$

This strategy is a common variance reduction strategy in Bayesian contexts (e.g., [Geweke, 1988](#)). The impact on the quality of the score estimator is shown in Figure 2.

#### 2.4.3. PERIODIC RESAMPLING STRATEGY

Since the variance of the estimator  $\hat{p}_t$  depends on  $p_{\text{is}}$ , which itself depends on the statistics of the ensemble  $\{\mathbf{x}_i\}$ , we can refine  $\hat{p}_t$  during the reverse diffusion by updating  $p_{\text{is}}$  using the statistics of  $\{\mathbf{x}_i\}$  at discrete resampling times,  $t_r$ , where  $0 < t_r < 1$ . After each resampling time,  $\hat{p}_t$  is held fixed until the next resampling time. By increasing the number of resampling times,  $N_r$ , during reverse diffusion,  $p_{\text{is}}$  is adapted to remain in the proximity of  $p_0$  during

the diffusion process, which prevents the likelihood ratio  $p_0(\mathbf{x}')/p_{\text{is}}(\mathbf{x}')$  from getting too small to effectively perform importance sampling (Agapiou et al., 2017). Importantly,  $p_0$  is only evaluated when updating  $\hat{p}_t$ , so there is a trade-off between increasing  $N_r$  to improve the score estimate while decreasing  $N_r$  to limit the total number of evaluations of  $p_0$ . For the experiments shown here,  $N_r$  is generally set to be between 10 and 30. Overall, this strategy is analogous in spirit to MCMC methods that utilize proposal distributions that adapt to the statistics of the Markov chains during sampling (e.g., Haario et al., 2001; Minson et al., 2013). The outline of this process is shown in Algorithm 1. By recomputing

---

**Algorithm 1** Resampling Strategy
 

---

**Input:** initial ensemble  $\mathbf{x}_i \in \mathbb{R}^D$ ,  $i \in \{1, \dots, N_{\text{ens}}\}$   
 mean vector  $\boldsymbol{\mu}$ , scaling matrix  $\mathbf{g}_t$   
 number of resampling steps  $N_r \Rightarrow \Delta t_r = \frac{1}{N_r}$   
 time step size  $\Delta t$   
**for**  $r = 1$  **to**  $N_r$  **do**  
   update  $p_{\text{is}}$  using  $\{\mathbf{x}_i\}_{i=1 \dots N_{\text{ens}}}$   
   update  $\hat{p}_t$  and hence  $\hat{\mathbf{s}}_t$  using antithetic samples  
    $t_{\text{start}} \leftarrow 1 - (r - 1)\Delta t_r$   
    $t_{\text{end}} \leftarrow 1 - r\Delta t_r$   
   **for**  $i = 1$  **to**  $N_{\text{ens}}$  **do**  
     solve reverse diffusion equation:  
      $\mathbf{x}_i \leftarrow \text{odesolve}(\mathbf{x}_i; t_{\text{start}}, t_{\text{end}}, \boldsymbol{\mu}, \mathbf{g}_t, \hat{\mathbf{s}}_t, \Delta t)$   
   **end for**  
**end for**  
**Return:**  $\{\mathbf{x}_i\}_{i=1 \dots N_{\text{ens}}}$

---

$p_{\text{is}}$  only periodically, we reduce the number of  $p_0$  evaluations, which is beneficial when  $p_0$  is expensive to evaluate. This situation is common in complex black box simulations settings where not only gradients are unavailable, but evaluations of the black box are also computationally expensive. As a result, we limit the number of forward evaluations in Algorithm 1 to a total of  $N_{\text{ens}}N_r$ . For example,  $N_r = 10$  resampling steps and an ensemble size  $N_{\text{ens}} = 100$  would result in 1000 evaluations of  $p_0$ .

## 2.5. Comparison with Ensemble Kalman Methods

Sampling and optimization methods based on Ensemble Kalman methods use an ensemble covariance matrix to estimate the gradient of a log probability density function that serves as the drift within a Langevin-type stochastic differential equation, see for example Garbuno-Inigo et al. (2020) for an easy-to-digest exposition. Usually, one can show that these methods become exact samplers in a Gaussian setting and convergence results can be obtained, for example, in convex and mean field settings (Schillings & Stuart, 2017; Garbuno-Inigo et al., 2020; Calvello et al., 2022). Score-based reverse diffusion samplers, as presented here, have the added advantage that they become exact sam-

Table 1. Parameters for the examples shown in Figure 1. For these experiments, the forward process has zero drift (i.e.,  $\mathbf{b}_t = \boldsymbol{\mu} = 0$ ), and the diffusion  $\mathbf{g}_t = (\sigma_{\text{min}}^{1/p} + t(\sigma_{\text{max}}^{1/p} - \sigma_{\text{min}}^{1/p}))^p$ , where  $p = 5$  (Karras et al., 2022). MIS here stands for the multiple importance sampling approach from Appendix E. Additionally,  $N_{\text{ens}} = 1000$ ,  $N_r = 10$ , and the initial time step size is specified by  $\Delta t_{\text{init}}$ .

DISTRIBUTION	$\sigma_{\text{min}}, \sigma_{\text{max}}$	$p_{\text{is}}$	$\Delta t_{\text{init}}$
BANANA	(0.01, 1)	MIXTURE (MIS)	0.005
RIDGED	(0.005, 1)	GAUSSIAN	0.005
MIXTURE	(0.005, 1)	GAUSSIAN	0.0025

plers for nearly any target distribution as the ensemble size and resampling times tend to infinity. However, score-based methods, as presented here, have the added disadvantage that they fight an uphill battle against the curse of dimensionality, discussed further in Sections 3.2 and 3.3. This situation is not surprising as estimating the score function in high dimensions using Monte Carlo sampling alone is a losing proposition because controlling the variance of the estimator becomes increasingly difficult.

## 3. Experiments

### 3.1. Low-dimensional Problems

We first apply our ensemble strategy to a set of two-dimensional Bayesian toy problems that exhibit posterior distributions with varying degrees of multimodality and non-ellipticity, which generally provide challenges to many MCMC techniques for sampling probability distributions. As shown in Figure 1, these problems include the well-known “banana”-shaped distribution, a distribution with neighboring high-probability ridges (adapted from Morzfeld et al. (2018)), and a mixture of three Gaussian distributions with well-separated means. The parameters used for each experiment are specified in Table 1. For comparison, we generate samples from these target distributions using three different techniques: 1) approximation of the distribution with a 2D multivariate Gaussian with parameters estimated via minimization of the reverse KL-divergence (i.e., variational inference (VI)); 2) NUTS; and 3) MALA.

As expected, the non-ellipticity of all three distributions present difficulties for methods that rely on or are related to Gaussian approximations. The reverse KL-divergence cost function used for VI encourages mode-seeking approximations, which can miss substantial areas of high probability for skewed or multi-modal distributions (Blei et al., 2017). Alternatively, both NUTS and MALA perform well for the “banana” distribution, but NUTS has a tendency to draw samples from a single mode or ridge of high probability, even when the ridges are not well-separated. MALA is most

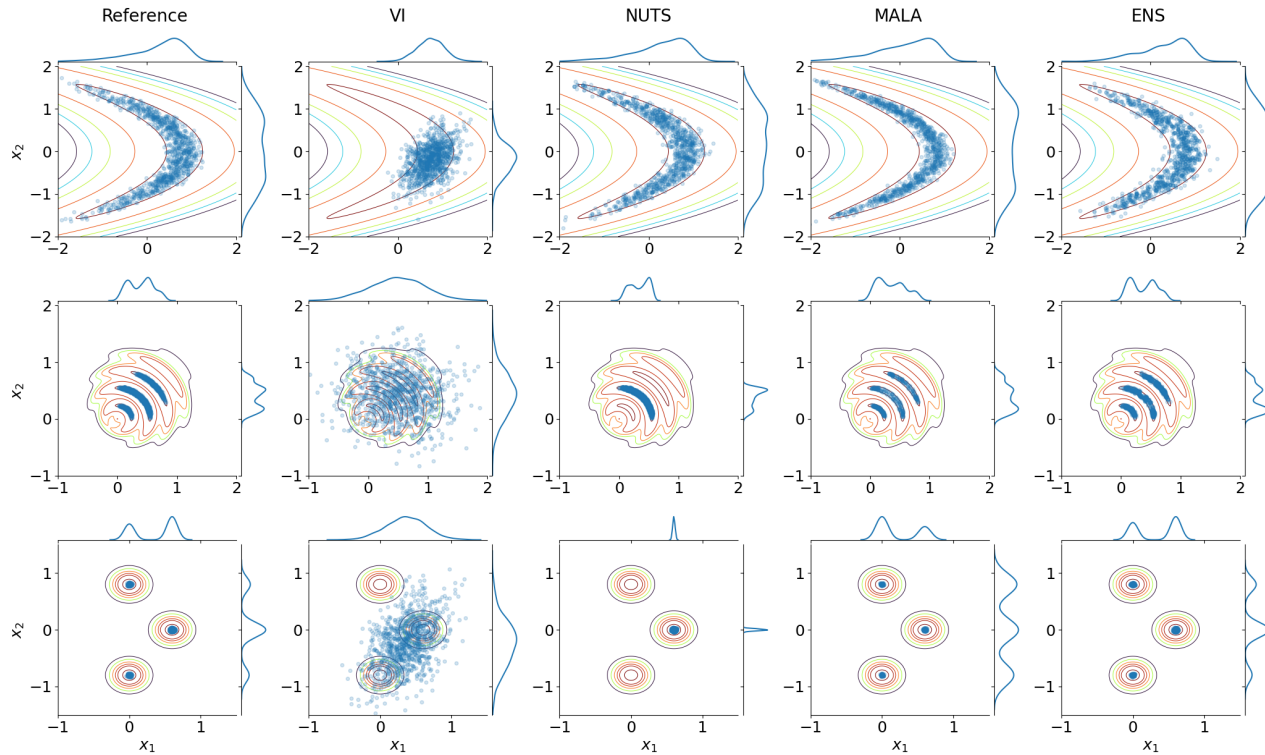


Figure 1. Comparison of different methods for drawing random samples from three different two-dimensional probability distributions. For each distribution, the joint plot shows contours of log probability along with the random samples while the marginal plots show kernel density estimates of the marginal distributions. The leftmost column shows direct samples from the distributions, while the rest of the columns represent samples from a variational inference approximation (VI), the No U-Turn Sampler (NUTS), a Metropolis-adjusted Langevin Algorithm (MALA), and the our approach (ENS).

similar to our method in that a diffusion process controls the random walk of samples that are initially randomly distributed, which permits samples to reach multiple regions of high probability. However, Langevin dynamics can suffer from slow mixing when modes are separated by low density regions, causing MALA to generate samples with incorrect relative densities for the mixture of Gaussians distribution (Song & Ermon, 2019). Our method is able to correctly sample all three distributions, demonstrating its ability to handle both non-ellipticity and multi-modality. We note that while a simple Metropolis-Hastings sampler could also accurately sample from these 2D distributions (with a large enough variance for the proposal distribution), it would quickly lose efficiency in higher dimensions. Our results broadly confirm the results obtained in Huang et al. (2021) where a Föllmer sampler was used to generate results from two-dimensional distributions, albeit their approach differs from ours in several ways (e.g., different Monte Carlo estimators, number of Monte Carlo samples, etc.)

### 3.1.1. INFLUENCE OF ENSEMBLE SIZE

As shown in Equations (6) and (7), the ensemble size affects the accuracy of the Monte Carlo estimate for the score function. Incorrect drift estimates will cause the sample trajectories to move toward incorrect locations in parameter space. In practice, the minimum ensemble size for sufficiently accurate drift estimates will depend on the dimensionality and “complexity” of the probability distribution. To explore this effect, we use our method to sample from a five-dimensional multivariate Gaussian distribution for different ensemble sizes. We quantify sample accuracy on the final ensembles generated by our method with an energy-based distance measurement that estimates the statistical distance between two sets of random vectors (Appendix B). We find that the energy distance of our method (measured between generated and reference samples from the 5- $d$  Gaussian) is reduced by a factor of three when increasing  $N_{\text{ens}}$  from 16 to 64, with a further factor of two reduction with  $N_{\text{ens}}$  from 64 to 256 (Figure 2). For smaller ensemble sizes, the antithetic sampling strategy can significantly decrease

sampling errors, while for larger ensembles, antithetic sampling can minimize the occurrence of high energy distances associated with inaccurate diffusion trajectories.

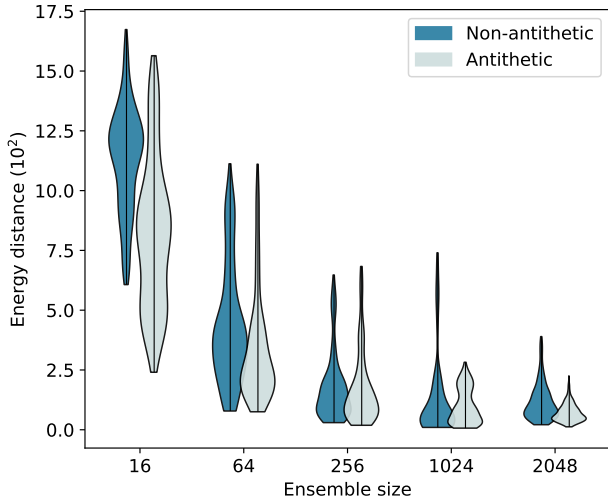


Figure 2. Violin plots showing energy distance between samples generated by our methods and ground truth samples from a 5- $d$  Gaussian as a function of ensemble size and dependent on whether an antithetic sampling strategy is used. At each ensemble size, energy distance was computed for 200 random permutations of the samples. The violin plots are bounded by the 10th and 90th percentiles of the resulting energy statistics.

### 3.2. Moderate-dimensional Problems

For low-dimensional problems ( $D < 10$ ), the linear operator  $\mathbf{b}_t$  and the scaling matrix  $\mathbf{g}_t$  in Equation (1) can be replaced with scalar terms such that the forward diffusion process evolves with equal variance in each dimension. As  $D$  increases, isotropic random walks can cause ensemble members to move to areas of low probability, similarly to the standard Metropolis-Hastings algorithm. One mitigation strategy is to convert the SDE in Equation (2) to a deterministic ODE (probability flow) (e.g., Song et al., 2021). In this way, the only source of randomness is in the initial ensemble, which is then evolved using only the drift term in Equation (2). However, since deterministic sampling continuously reduces noise levels during reverse diffusion (Karras et al., 2022), the final samples may undersample  $p_0$  and collapse to local modes. Moreover, another challenge with larger  $D$  is that the fraction of initial ensemble members  $\{x_i\}$  within low-probability regions of  $p_0$  quickly approaches 1, which results in inaccurate Monte Carlo estimates of the score function and resulting drift.

For certain classes of problems where some information about the covariance structure of the parameters is available

a priori, we can employ a localization-type strategy. Specifically, the flexible form of Equation (1) allows us to choose the scaling matrix of the forward diffusion to be a localization matrix defined as the Cholesky-decomposed prior covariance. In other words, by defining a forward diffusion process that utilizes the prior covariance, we can “push” the diffusion process to stay “close” to the dominant subspace defined by the prior covariance. The implicit assumption is that the posterior will follow a similar covariance structure as defined by the prior. In essence, this localization strategy is a kind of linear dimensionality reduction strategy where we assume that we know the relevant subspace a priori (e.g., Webber & Morzfeld, 2023). As a result, this strategy becomes more useful as the dimensionality of the problem increases. In the examples presented here, we utilize an Ornstein-Uhlenbeck forward process for the forward diffusion process with drift and diffusion operators defined as

$$\mathbf{b}_t = \theta(\boldsymbol{\mu} - \mathbf{x}_t), \quad (10a)$$

$$\mathbf{g}_t = \text{Cholesky}(\alpha \boldsymbol{\Sigma}_{\text{prior}}), \quad (10b)$$

which evolves samples from  $p_0$  to a multivariate Gaussian distribution  $\mathcal{N}(\boldsymbol{\mu}, \alpha \boldsymbol{\Sigma}_{\text{prior}})$  over a time scale  $\theta > 0$ . Here,  $\alpha$  is a scalar inflation factor for scaling the prior covariance in order to optionally inflate the initial ensemble. We chose the magnitude of  $\theta$  such that as  $t \rightarrow 1$  the process has converged to  $\mathcal{N}(\boldsymbol{\mu}, \alpha \boldsymbol{\Sigma}_{\text{prior}})$  in a distributional sense. The reverse diffusion process can then be determined by simply plugging  $\mathbf{b}_t$  and  $\mathbf{g}_t$  into Equation 2. We apply this strategy to a 20-dimensional Bayesian linear regression problem. The regression problem corresponds to estimating the coefficients,  $\mathbf{x} \in \mathbb{R}^{20}$ , of uniformly spaced B-splines placed in the columns of a linear operator  $\mathbf{G} \in \mathbb{R}^{500 \times 20}$ , given a data vector  $\mathbf{d} \in \mathbb{R}^{500}$  (Appendix C). The B-splines serve as smooth interpolating basis functions for reconstructing signals from noisy data. In this class of regression problems, it is common to enforce a prior constraint that the spline coefficients are correlated over a given length scale, which can be represented by a squared-exponential Gaussian Process kernel  $k(x_i, x_j) = \exp[-d(x_i, x_j)^2 / (2L^2)]$ , where  $d(x_i, x_j)$  is the Euclidean distance and  $L$  is the prescribed length scale (e.g., Jolivet et al., 2014; Webber & Morzfeld, 2023). Using this kernel to build the scale matrix  $\mathbf{g}_t$  for the Ornstein-Uhlenbeck forward process (see Table 2 for full parameter specification), we are able to obtain samples from the target posterior distribution that have nearly the same accuracy as methods that utilize gradients of the log posterior, see Figure 3.

### 3.3. High-dimensional Problems

For this example, we aim to estimate a permeability field,  $a(\mathbf{x})$ , that leads to an observed pressure field,  $P(\mathbf{x})$ , in a porous medium resulting from a scalar field of fluid sources

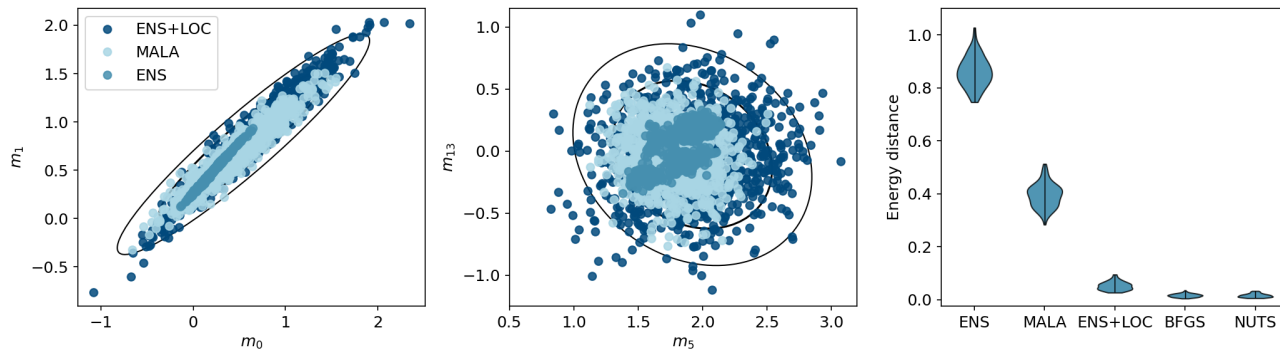


Figure 3. **Marginal posterior samples** and **energy distance** for different sampling methods for the 20- $d$  Bayesian linear regression. For the marginal plots (left and center), the outer ellipse represents the  $3\sigma$  posterior uncertainty as computed by the analytic least squares solution. Energy distance (right) is computed relative to the least squares solution. Ensemble methods (ENS) without a localization strategy can successfully find the mode of the posterior, but significantly underestimate the posterior variance. When using an Ornstein-Uhlenbeck forward process (ENS+LOC) based on the prior distribution, posterior samples are drawn at a comparable accuracy to methods that require gradients of the log posterior. For ENS, we use a probability flow with  $(\sigma_{\min}, \sigma_{\max}) = (0.1, 10)$  and  $\mathbf{g}_t$  with the form in Table 1. The ENS+LOC parameters are specified in Table 2. BFGS samples for computing the energy distance were generated from the Hessian approximation.

Table 2. Parameters for the 20- $d$  and 100- $d$  problems utilizing the Ornstein-Uhlenbeck forward process with localization based on the prior covariance. For both problems, we set  $N_{\text{ens}} = 1000$ .

PROBLEM	$\theta$	$\mu$	$\alpha$	$\Delta t_{\text{init}}$	$N_r$
20- $d$	0.1	0	$4^2$	0.002	10
100- $d$	0.05	0	$5^2$	0.002	30

or sinks,  $f(\mathbf{x})$ . This system is governed by a partial differential equation (PDE) involving spatial gradients of  $a(\mathbf{x})$  and  $P(\mathbf{x})$  (see Appendix D). In this simplified experiment, we start with dense, noisy observations of  $P(\mathbf{x})$  and assume that  $f(\mathbf{x})$  is known. The inverse problem becomes estimating  $a(\mathbf{x})$  such that the force balance described by the PDE in Appendix D is satisfied. This formulation allows for straightforward comparison with MCMC methods that leverage gradient information without having to back-propagate through a numerical solver. We model  $a(\mathbf{x})$  as a linear combination of two-dimensional B-splines such that  $a(\mathbf{x}) = \mathbf{G}(\mathbf{x})\mathbf{m}$ , where  $\mathbf{G}(\mathbf{x})$  is the spline matrix and  $\mathbf{m} \in \mathbb{R}^{100}$  (Appendix D).

Using the insights from the previous section, we apply our ensemble method with an Ornstein-Uhlenbeck forward process (Table 2) to sample from the posterior distribution of the spline coefficients, where the scaling matrix of the diffusion process is defined by the Cholesky-decomposed covariance matrix of the prior distribution. The prior covariance is constructed to encourage a smooth reconstruction of the permeability field. Compared with samples obtained from

NUTS and MALA, our method successfully samples from the posterior distribution, although, similar to MALA, the samples exhibit slightly lower variance than those obtained with NUTS, see Figure 4. This effect is likely driven by the relative weakness in the correlations (off-diagonal terms) of the prior covariance matrix used in the Ornstein-Uhlenbeck forward process, which in turn provides weaker constraints on the ensemble random walk during reverse diffusion. As a result, the likelihood ratio  $p_0(\mathbf{x}')/p_{\text{is}}(\mathbf{x}')$  in Equation (6) becomes dominated by a small subset of the ensemble members, causing the other members to drift towards that subset. We find this effect to be more pronounced when using scalar (isotropic) diffusion processes. Nevertheless, our ensemble method with the Ornstein-Uhlenbeck forward process is successfully able to sample a substantial region of the posterior distribution in high-dimensions without requiring gradients of the distribution.

## 4. Conclusions

In this study, we introduced the ensemble strategies that leverage the dynamics of particle ensembles to estimate a score function used to generate samples from a target distributions within a reverse diffusion process. This method, rooted in principles of importance sampling, is robust for low- to medium-dimensional problems where gradients of the posterior log probability or the forward model are unavailable. This is often the case for complex black box forward models where analytic gradients are intractable and automatic differentiation methods are not an option.

Our experiments, encompassing a hierarchy of problems,

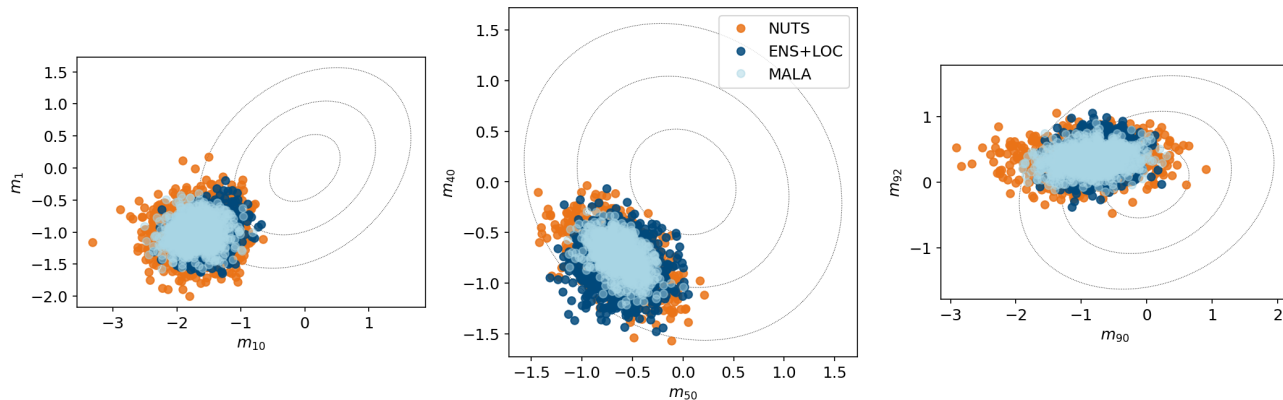


Figure 4. **Marginal posterior samples** for select pairs of two-dimensional B-splines used to reconstruct a permeability field given observations of a pressure field. Our ensemble method with an Ornstein-Uhlenbeck localization process (ENS+LOC) is compared to NUTS and MALA. The ellipses in each plot correspond to the prior covariance (1-, 2-, and 3- $\sigma$ ). For this 100- $d$  problem, the posterior samples obtained with ENS+LOC are similar to those obtained with the gradient-based NUTS and MALA.

highlight the advantages of our method over traditional MCMC methods such as NUTS and MALA, even when these methods use gradient information. Particularly noteworthy is the ability to effectively navigate and sample from non-Gaussian distributions, which makes this approach an appealing choice especially in fields like geophysics and computational physics where such challenges are prevalent.

Furthermore, the implementation of resampling strategies has substantially enhanced the computational efficiency of this method when compared to related gradient-free strategies such as vanilla Föllmer sampling. The adaptability of our method to various problem sizes and its ability to integrate domain-specific knowledge (e.g., using prior covariances in geophysical applications) further underscore its practical utility.

The ideas presented here are however not without challenges and warrant further investigation. The scalability to very high-dimensional problems remains a challenge that is rooted in the obvious curse of dimensionality. While our strategy of utilizing Ornstein-Uhlenbeck processes defined by prior information has shown promise, additional research is needed to optimize for such scenarios. In other Bayesian inference scenarios, priors may be relatively uninformative, which could limit the utility of the Ornstein-Uhlenbeck processes. Other works have approached this problem by training neural network models of the score, but those methods require taking gradients of the log posterior. It remains a challenge to build a completely gradient-free method that also works in high dimensions while remaining computationally efficient.

## Software and Data

We implemented all algorithms and strategies presented in this work in JAX (Bradbury et al., 2018). In particular, we used the Equinox (Kidger & Garcia, 2021) and DiffraX (Kidger, 2022) packages to build a flexible implementation of forward-reverse diffusion systems.

## Broader Impact

This paper presents work whose goal is to advance the field of Machine Learning. There are many potential societal consequences of our work, none which we feel must be specifically highlighted here.

## References

- Agapiou, S., Papaspiliopoulos, O., Sanz-Alonso, D., and Stuart, A. M. Importance sampling: Intrinsic dimension and computational cost. *Statistical Science*, pp. 405–431, 2017.
- Anderson, B. D. Reverse-time diffusion equation models. *Stochastic Processes and their Applications*, 12(3):313–326, 1982.
- Blei, D. M., Kucukelbir, A., and McAuliffe, J. D. Variational inference: A review for statisticians. *Journal of the American statistical Association*, 112(518):859–877, 2017. doi: <https://doi.org/10.1080/01621459.2017.1285773>.
- Boffi, N. M. and Vanden-Eijnden, E. Probability flow solution of the Fokker–Planck equation. *Machine Learning: Science and Technology*, 4(3):035012, 2023. doi: [10.1088/2632-2153/ace2aa](https://doi.org/10.1088/2632-2153/ace2aa).



- Bortoli, V. D., Thornton, J., Heng, J., and Doucet, A. Diffusion schrödinger bridge with applications to score-based generative modeling, 2023.
- Bradbury, J., Frostig, R., Hawkins, P., Johnson, M. J., Leary, C., Maclaurin, D., Necula, G., Paszke, A., VanderPlas, J., Wanderman-Milne, S., and Zhang, Q. JAX: composable transformations of Python+NumPy programs, 2018. URL <http://github.com/google/jax>.
- Bunne, C., Hsieh, Y.-P., Cuturi, M., and Krause, A. Recovering Stochastic Dynamics via Gaussian Schrödinger Bridges. *arXiv*, 2022. doi: 10.48550/arxiv.2202.05722.
- Calvello, E., Reich, S., and Stuart, A. M. Ensemble kalman methods: A mean field perspective, 2022.
- Chada, N. K. A review of the EnKF for parameter estimation, 2022.
- Dai, Y., Jiao, Y., Kang, L., Lu, X., and Yang, J. Z. Global Optimization via Schrödinger-Föllmer Diffusion. *arXiv*, 2021. doi: 10.48550/arxiv.2111.00402.
- Elvira, V. and Martino, L. Advances in importance sampling, 2022.
- Föllmer, H. An entropy approach to the time reversal of diffusion processes. In *Stochastic Differential Systems Filtering and Control*, pp. 156–163. Springer, 1985.
- Föllmer, H. Time reversal on wiener space. In *Stochastic processes—mathematics and physics*, pp. 119–129. Springer, 1986.
- Garbuno-Inigo, A., Hoffmann, F., Li, W., and Stuart, A. M. Interacting langevin diffusions: Gradient structure and ensemble kalman sampler. *SIAM Journal on Applied Dynamical Systems*, 19(1):412–441, 2020. doi: <https://doi.org/10.1137/19M1251655>.
- Gardiner, C. W. et al. *Handbook of stochastic methods*, volume 3. springer Berlin, 1985.
- Geweke, J. Antithetic acceleration of monte carlo integration in bayesian inference. *Journal of Econometrics*, 38 (1-2):73–89, 1988.
- Haario, H., Saksman, E., and Tamminen, J. An adaptive metropolis algorithm. *Bernoulli*, 7(2):223–242, 2001.
- Ham, D. A., Kelly, P. H. J., Mitchell, L., Cotter, C. J., Kirby, R. C., Sagiya, K., Bouziani, N., Vorderwuelbecke, S., Gregory, T. J., Betteridge, J., Shapero, D. R., Nixon-Hill, R. W., Ward, C. J., Farrell, P. E., Brubeck, P. D., Marsden, I., Gibson, T. H., Homolya, M., Sun, T., McRae, A. T. T., Luporini, F., Gregory, A., Lange, M., Funke, S. W., Rathgeber, F., Bercea, G.-T., and Markall, G. R. *Firedrake User Manual*. Imperial College London and University of Oxford and Baylor University and University of Washington, first edition edition, 5 2023.
- Hetland, E., Musé, P., Simons, M., Lin, Y., Agram, P., and DiCaprio, C. Multiscale InSAR time series (MInTS) analysis of surface deformation. *Journal of Geophysical Research: Solid Earth*, 117(B2), 2012. doi: 10.1029/2011JB008731.
- Hoffman, M. D., Gelman, A., et al. The No-U-Turn sampler: adaptively setting path lengths in hamiltonian monte carlo. *J. Mach. Learn. Res.*, 15(1):1593–1623, 2014.
- Huang, J., Jiao, Y., Kang, L., Liao, X., Liu, J., and Liu, Y. Schrödinger-Föllmer sampler: sampling without ergodicity. *arXiv preprint arXiv:2106.10880*, 2021. doi: <https://doi.org/10.48550/arXiv.2106.10880>.
- Jiao, Y., Kang, L., Liu, Y., and Zhou, Y. Convergence Analysis of Schrödinger-Föllmer Sampler without Convexity. *arXiv*, 2021. doi: 10.48550/arxiv.2107.04766.
- Jolivet, R., Duputel, Z., Riel, B., Simons, M., Rivera, L., Minson, S. E., Zhang, H., Aivazis, M. A. G., Ayoub, F., Leprince, S., Samsonov, S., Motagh, M., and Fielding, E. J. The 2013 Mw 7.7 Balochistan Earthquake: Seismic Potential of an Accretionary Wedge. *Bulletin of the Seismological Society of America*, 104(2):1020–1030, 03 2014. ISSN 0037-1106. doi: 10.1785/0120130313.
- Karras, T., Aittala, M., Aila, T., and Laine, S. Elucidating the design space of diffusion-based generative models. *Advances in Neural Information Processing Systems*, 35: 26565–26577, 2022.
- Kidger, P. On neural differential equations, 2022.
- Kidger, P. and Garcia, C. Equinox: neural networks in jax via callable pytrees and filtered transformations, 2021.
- Minson, S. E., Simons, M., and Beck, J. L. Bayesian inversion for finite fault earthquake source models I—theory and algorithm. *Geophysical Journal International*, 194 (3):1701–1726, 06 2013. ISSN 0956-540X. doi: 10.1093/gji/ggt180.
- Morzfeld, M., Day, M. S., Grout, R. W., Heng Pau, G. S., Finsterle, S. A., and Bell, J. B. Iterative importance sampling algorithms for parameter estimation. *SIAM Journal on Scientific Computing*, 40(2):B329–B352, 2018. doi: <https://doi.org/10.1137/16M1088417>.
- Raissi, M., Perdikaris, P., and Karniadakis, G. E. Physics-informed neural networks: A deep learning framework for solving forward and inverse problems involving nonlinear partial differential equations. *Journal of Computational physics*, 378:686–707, 2019. doi: 10.1016/j.jcp.2018.10.045.

- Ramos-Carreño, C. and Torrecilla, J. L. dcor: Distance correlation and energy statistics in Python. *SoftwareX*, 22, 2 2023. doi: 10.1016/j.softx.2023.101326.
- Reich, S. Data assimilation: The Schrödinger perspective. *Acta Numerica*, 28:635–711, 2019. ISSN 0962-4929. doi: 10.1017/s0962492919000011.
- Roberts, G. O. and Tweedie, R. L. Exponential convergence of langevin distributions and their discrete approximations. *Bernoulli*, pp. 341–363, 1996. doi: <https://doi.org/10.2307/3318418>.
- Schillings, C. and Stuart, A. Convergence analysis of ensemble kalman inversion: The linear, noisy case, 2017.
- Schrödinger, E. Sur la théorie relativiste de l'électron et l'interprétation de la mécanique quantique. In *Annales de l'institut Henri Poincaré*, volume 2, pp. 269–310, 1932.
- Song, Y. and Ermon, S. Generative modeling by estimating gradients of the data distribution. In Wallach, H., Larochelle, H., Beygelzimer, A., d'Alché-Buc, F., Fox, E., and Garnett, R. (eds.), *Advances in Neural Information Processing Systems*, volume 32. Curran Associates, Inc., 2019.
- Song, Y., Sohl-Dickstein, J., Kingma, D. P., Kumar, A., Ermon, S., and Poole, B. Score-based generative modeling through stochastic differential equations, 2021.
- Székely, G. J. and Rizzo, M. L. Energy statistics: A class of statistics based on distances. *Journal of Statistical Planning and Inference*, 143(8):1249–1272, 2013. ISSN 0378-3758. doi: <https://doi.org/10.1016/j.jspi.2013.03.018>.
- Tarantola, A. *Inverse problem theory and methods for model parameter estimation*. SIAM, 2005.
- Vargas, F., Ovsianas, A., Fernandes, D., Girolami, M., Lawrence, N. D., and Nüsken, N. Bayesian learning via neural Schrödinger–Föllmer flows. *Statistics and Computing*, 33(1):3, 2023. ISSN 0960-3174. doi: 10.1007/s11222-022-10172-5.
- Webber, R. J. and Morzfeld, M. Localized covariance estimation: A Bayesian perspective, 2023.
- Zhang, Q. and Chen, Y. Path integral sampler: a stochastic control approach for sampling, 2022.

## A. Anisotropic Forward Diffusion

For higher-dimensional problems where some information on the covariance structure of the target distribution is available (which is common for geophysical systems, due to physical constraints), Ornstein-Uhlenbeck processes with non-zero drift coefficients and with diffusion informed by the known covariance structure (Equation 10) can significantly improve the accuracy of the reverse diffusion process. For scalar Brownian motion, the samples will take random walks in each dimension with equal variance. For higher-dimensional problems, this behavior can cause many samples to move towards low probability regions of the target distribution. With the Ornstein-Uhlenbeck process, the random walks are constrained to the covariance structure imposed by  $\mathbf{g}_t$ , which for certain problems can keep samples in the relevant regions of the probability space to improve the estimate of the Föllmer drift (Figure 5). In practice, we also tune  $\theta$  to control the relative importance of  $\mu$  during the reverse diffusion. For  $\theta = 1$ , the samples will stay close to  $\mu$ , which can be un-desirable when the target mean is expected to differ non-negligibly from  $\mu$ . For the higher-dimensional experiments in this work, we find  $\theta = 0.1 - 0.2$  to provide the best accuracy.

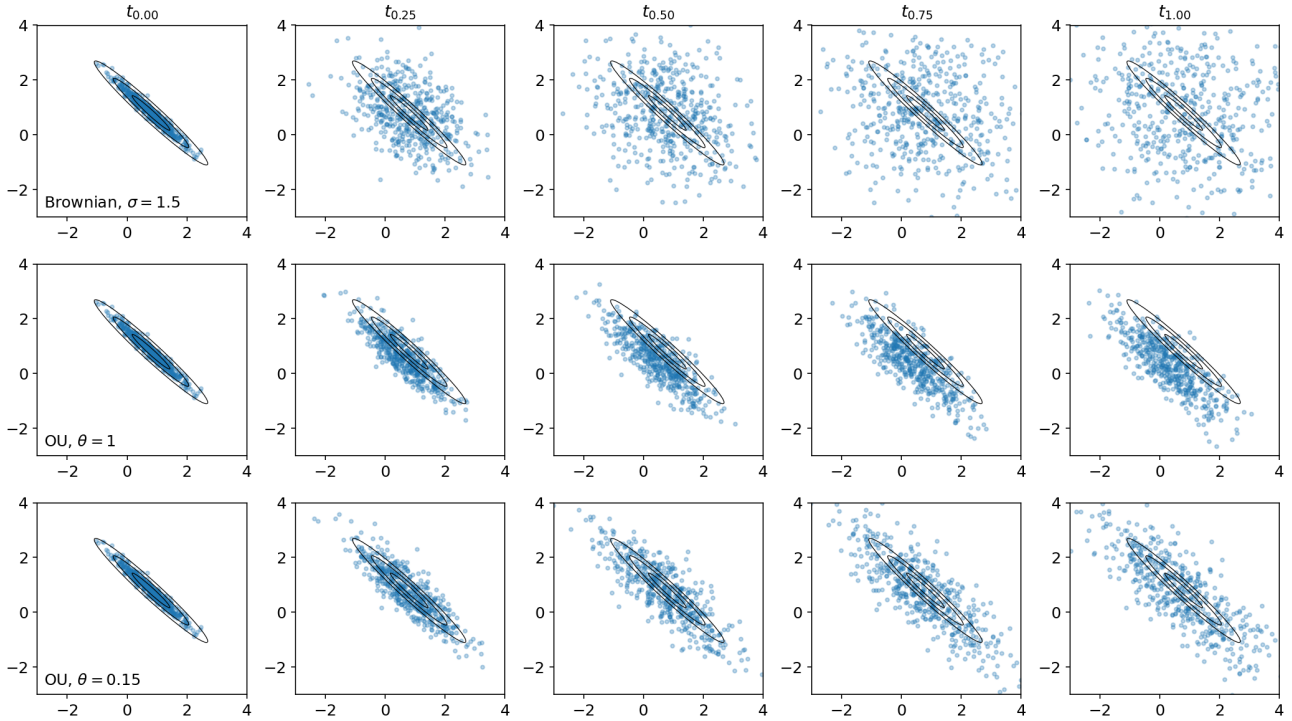


Figure 5. Simulated forward diffusion for different functional forms of the forward process. The initial sample ( $t_{0.00}$ , left) is generated from a multivariate Gaussian with  $\mu_0 = [0.8, 0.8]$  and  $\Sigma_0 = [[0.4, -0.39], [-0.39, 0.4]]$ . **Top:** Brownian process with zero drift and  $\sigma = 1.5$ . **Middle:** Ornstein-Uhlenbeck process with  $\theta = 1$ ,  $\mu = 0$ , and  $\Sigma = [[0.5, -0.4], [-0.4, 0.5]]$ . **Bottom:** Same as the middle Ornstein-Uhlenbeck process but with  $\theta = 0.15$ .

## B. Energy distance

The energy distance  $\epsilon$  is related to the covariance distance between two random vectors  $\mathbf{X}$  and  $\mathbf{Y}$  and is defined as (Székely & Rizzo, 2013):

$$\epsilon(\mathbf{X}, \mathbf{Y}) = 2\mathbb{E}(\|\mathbf{X} - \mathbf{Y}\|_p) - \mathbb{E}(\|\mathbf{X} - \mathbf{X}'\|_p) - \mathbb{E}(\|\mathbf{Y} - \mathbf{Y}'\|_p), \quad (11)$$

where  $\|\cdot\|_p$  is the  $p$ -norm and  $\mathbf{X}'$  and  $\mathbf{Y}'$  are random permutations of  $\mathbf{X}$  and  $\mathbf{Y}$ , respectively. As such, the estimate for  $\epsilon(\mathbf{X}, \mathbf{Y})$  can be repeated for multiple realizations of  $\mathbf{X}'$  and  $\mathbf{Y}'$  such that the mean value represents a more robust estimate. Here, we use the Python package `dcop` package to compute  $\epsilon(\mathbf{X}, \mathbf{Y})$  (Ramos-Carreño & Torrecilla, 2023). As

this estimate can vary depending on the size of the vectors  $\mathbf{X}$  and  $\mathbf{Y}$ , comparing the samples generated by our method for different ensemble sizes requires multiple runs of our method with different initial random ensembles until a vector of a fixed size  $N_{\text{total}}$  is filled, where  $N_{\text{total}}$  is several multiples of  $N_{\text{ens}}$ . Overall, we find the energy distance to be a robust way of comparing samples from arbitrary probability distributions, and we find that using a  $p$ -norm with  $p = 1$  or  $1.5$  can mitigate the effects of outliers in  $\mathbf{X}$  and  $\mathbf{Y}$ .

### C. Bayesian linear regression

For the linear model used in Section 3.2, the matrix  $\mathbf{G}$  is constructed from 20 equally-sized B-splines uniformly distributed along some spatial dimension (Figure 6a.) (Hetland et al., 2012). The spline coefficients, represented by the vector  $\mathbf{x}$ , are

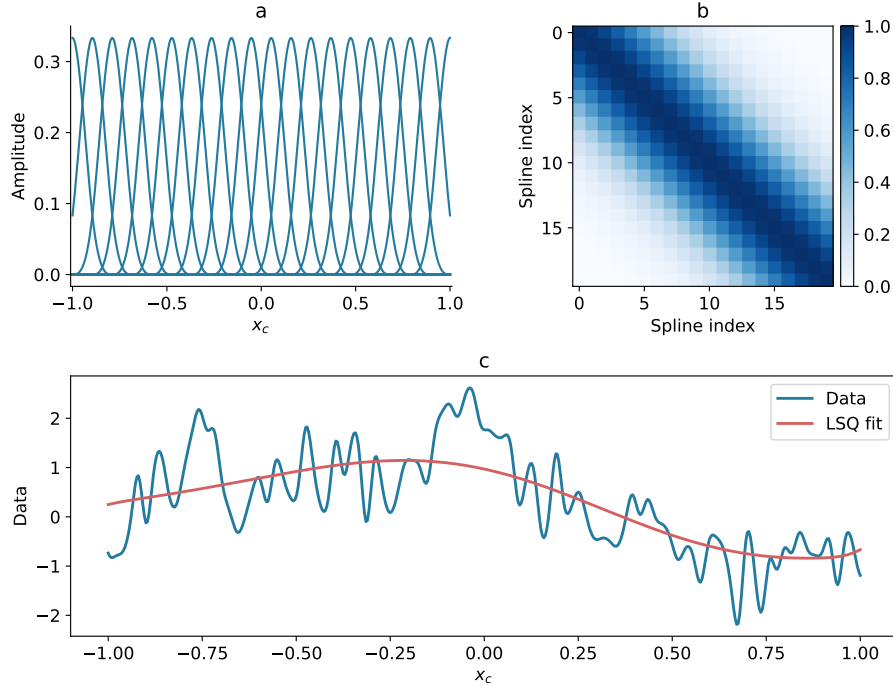


Figure 6. **Top left (a):** B-splines used in the Bayesian linear regression example from Section 3.2. **Top right (b):** Prior covariance of spline coefficients in Bayesian linear regression example. **Bottom (c):** Synthetic noisy data and corresponding least squares fit used for reference solution.

assumed to be spatially correlated following the prior covariance structure shown in Figure 6b, which is constructed from the squared-exponential Gaussian Process kernel as described in Section 3.2. In this experiment, the B-splines are defined within a spatial domain of  $[-1, 1]$ , and the prior length scale  $L$  is set to 0.5.

The posterior distribution for the spline coefficients follows from Bayes' Theorem (ignoring the normalization constant):

$$p(\mathbf{x}|\mathbf{d}) \sim p(\mathbf{d}|\mathbf{x})p(\mathbf{x}), \quad (12)$$

where the first distribution on the right-hand side is the likelihood distribution and the second distribution is the prior distribution. For a given data vector  $\mathbf{d} = \mathbf{G}\mathbf{x} + \epsilon$ , where  $\epsilon \sim \mathcal{N}(\mathbf{0}, \sigma_d^2 \mathbf{I})$  is normally distributed noise with variance  $\sigma_d$ , and a multivariate Gaussian prior,  $p(\mathbf{x}) \sim \mathcal{N}(\mathbf{0}, \Sigma_{\text{prior}})$ , we can derive an analytic solution for  $p(\mathbf{x}|\mathbf{d})$  as the least-squares estimate (Tarantola, 2005):

$$\hat{\mathbf{x}} = \left( \mathbf{G}^T \mathbf{G} + \sigma_d^2 \Sigma_{\text{prior}}^{-1} \right)^{-1} \mathbf{G}^T \mathbf{d}. \quad (13)$$

The corresponding posterior covariance matrix for  $\hat{\mathbf{x}}$  is

$$\Sigma_{\hat{\mathbf{x}}} = \sigma_d^2 \left( \mathbf{G}^T \mathbf{G} + \sigma_d^2 \Sigma_{\text{prior}}^{-1} \right)^{-1}. \quad (14)$$

Together,  $\hat{\mathbf{x}}$  and  $\Sigma_{\hat{\mathbf{x}}}$  are used to construct a reference multivariate Gaussian distribution to compare the various sampling methods. For this experiment, we generate  $\mathbf{d}$  by sampling a reference  $\mathbf{x}$  from a unit Gaussian distribution and multiplying by  $G$ . We additionally add noise with a length scale of 0.05 and a variance of  $\sigma_d = 2.0$  to obtain the final  $\mathbf{d}$  used in the experiments.

## D. Darcy Flow

For a spatial domain defined by coordinates  $\mathbf{x}$ , a permeability field,  $a(\mathbf{x})$ , and a scalar field of fluid sources or sinks,  $f(\mathbf{x})$ , the following PDE can be derived for a pressure field  $P(\mathbf{x})$  following the derivation of Darcy flow (e.g., Garbuno-Inigo et al., 2020):

$$-\nabla \cdot (a(\mathbf{x})\nabla P(\mathbf{x})) = f(\mathbf{x}), \quad \mathbf{x} \in \mathcal{D}, \quad (15a)$$

$$P(\mathbf{x}) = 0, \quad \mathbf{x} \in \partial\mathcal{D}, \quad (15b)$$

where  $\mathcal{D}$  represents the interior of the modeling domain and  $\partial\mathcal{D}$  represents the boundary. We prescribe  $\mathcal{D}$  to span the domain  $[0, 1]^2$  and assume that all fields have normalized units. We solve the above equations for a unit square mesh with Dirichlet boundary conditions using `firedrake` (Ham et al., 2023). The ground truth  $a(\mathbf{x})$  is modeled as  $a(\mathbf{x}) = a_0 e^{\theta(\mathbf{x})}$ , where  $a_0 = 0.6$  and  $\theta(\mathbf{x})$  is a random Gaussian field with a length scale of 0.15. The simulated fields are shown in Figure 7.

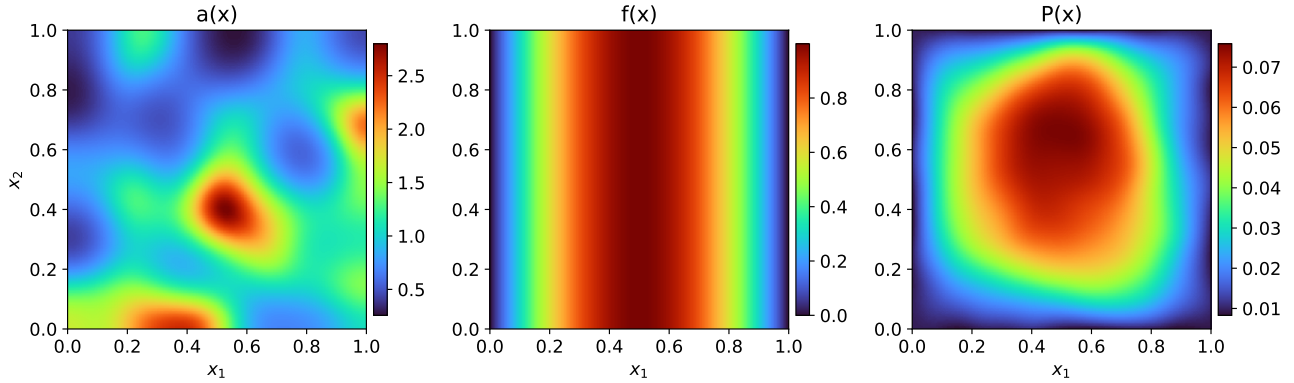


Figure 7. Spatial fields with normalized units used in the pressure field PDE. The permeability field (a) and source field (b) lead to the pressure field (c) following Equation 15a. Noise with a standard deviation of 0.001 is added to the pressure field.

The inverse problem aims to recover  $\theta(\mathbf{x})$ , which ensures that  $a(\mathbf{x})$  is strictly positive. We simplify the problem by assuming that both  $f(\mathbf{x})$  and  $P(\mathbf{x})$  are known, where the former is prescribed and the latter is computed with `firedrake` as stated above. The forward problem then becomes taking  $a(\mathbf{x})$  as input into Equation (15a) and computing the residual force balance, i.e.:

$$\mathbf{r} = f(\mathbf{x}) + \nabla \cdot (a(\mathbf{x})\nabla P(\mathbf{x})). \quad (16)$$

In other words, we aim to estimate  $a(\mathbf{x})$  that minimizes the force balance residual, which is a strategy widely used in physics-informed machine learning (e.g., Raissi et al., 2019). This approach removes the need for backpropagating through a numerical solver and facilitates comparison of our approach with methods that require gradients through the log posterior of  $\theta(\mathbf{x})$ . Each spatial field is resampled to a  $100 \times 100$  square grid such that the gradients in Equation (15a) can be evaluated with finite differences.

However, the uniform grid still results in 10,000 grid cells. In order to reduce the dimensionality of the spatial fields for the inverse problem, we represent the fields as a linear combination of 100 2D B-splines distributed uniformly in both the horizontal and vertical directions (Figure 8). The two-dimensional B-splines are simple outer products of the one-dimensional B-splines used in the linear regression problem and can decompose spatial fields in a manner similar to wavelet transforms. Splines of multiple length scales can be combined in order to accurately represent multiscale fields.

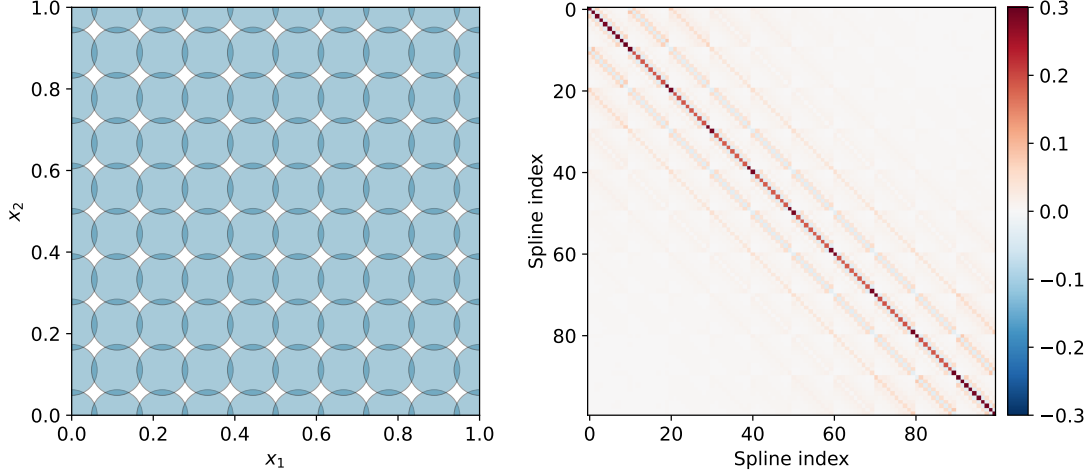


Figure 8. **Left:** Illustration of the location and approximate supports for the 2D B-splines used for decomposing spatial fields. **Right:** Prior covariance matrix based on the Laplacian operator on the spline coefficients.

Here, we simply use a single length scale for our analysis. Each spline is evaluated on the same  $100 \times 100$  square grid as the pressure and source fields, flattened to a column vector, and placed into a column of a matrix  $\mathbf{G} \in \mathbb{R}^{10000 \times 100}$ . The posterior distribution for the spline coefficient vector,  $\mathbf{m}$ , is (here we use  $\mathbf{m}$  to avoid confusion with the coordinate space defined by  $\mathbf{x}$ ):

$$p(\mathbf{m}|\mathbf{r}) \sim p(\mathbf{r}|\mathbf{m})p(\mathbf{m}). \quad (17)$$

In this experiment, we prescribe the likelihood  $p(\mathbf{r}|\mathbf{m})$  as a Laplace distribution  $\mathbf{r} = \mathcal{L}(0, b_r)$  where  $b_r = 5.4$  is the scale parameter. The Laplace distribution permits a longer tail of  $\mathbf{r}$  values while also providing a demonstration of Bayesian inference with non-Gaussian distributions. The prior distribution is represented as a multivariate Gaussian with a zero mean vector and a covariance matrix  $\Sigma_{\text{prior}}$ . While the prior covariance can again be constructed with the squared-exponential Gaussian Process kernel to enforce a correlation length scale, we choose to instead construct a Laplacian smoothing matrix that estimates the 2nd-derivative of the spline coefficients in both directions (Figure 8). This matrix format is well-suited to sparse representations, which can improve computational efficiency in higher dimensions, while still encouraging a spatially smooth  $\theta(\mathbf{x})$ . The spatial gradient of each spline in  $\mathbf{G}$  is computed with finite differences in both directions, e.g.  $\mathbf{G}_x$  and  $\mathbf{G}_y$  are matrices containing the  $x$ - and  $y$ - gradients of the splines in their columns. The prior covariance is then computed as

$$\Sigma_{\text{prior}} = \lambda(\mathbf{G}_x^T \mathbf{G}_x + \mathbf{G}_y^T \mathbf{G}_y) + \sigma_p^2 \mathbf{I}, \quad (18)$$

where  $\lambda$  is a scalar smoothing penalty and  $\sigma_p^2 \mathbf{I}$  is an additive prior on the spline amplitudes. Here, we set  $\lambda = 0.001$  and  $\sigma_p = 1$ .

## E. Multiple Importance Sampling Approach

An alternative to the simple Gaussian importance sampling distribution  $p_{\text{is}}$  from Section 2.4.1 is to use a multiple importance sampling strategy (e.g., Elvira & Martino, 2022), where each component is a Gaussian centered on the location of an ensemble member. The multiple importance sampling estimator of  $p_t$  is then given by

$$\hat{p}_t(\mathbf{x}) = \sum_{i=1}^{N_{\text{ens}}} \frac{1}{N_i} \sum_{j=1}^{N_i} \kappa_t(\mathbf{x}|\mathbf{x}'_{ij}) w_i(\mathbf{x}'_{ij}) \frac{p_0(\mathbf{x}'_{ij})}{p_{\text{is},i}(\mathbf{x}'_{ij})}, \quad \mathbf{x}'_{ij} \sim p_{\text{is},i}, \quad (19)$$

where  $N_i$  is the number of samples drawn for component  $i$ . By choosing  $p_{\text{is},i}(\mathbf{x}) = \kappa_t(\mathbf{x}|\mathbf{x}_i)$ , where  $\mathbf{x}_i$  is an ensemble member (e.g., a sample in the process of being generated by the reverse diffusion process from Equation (2)), and by computing  $w_i$  using the balance heuristic (Elvira & Martino, 2022)

$$w_i(\mathbf{x}) = \frac{N_i \kappa_t(\mathbf{x}|\mathbf{x}_i)}{\sum_{j=1}^{N_{\text{ens}}} N_j \kappa_t(\mathbf{x}|\mathbf{x}_j)}, \quad (20)$$

one can assemble a multiple importance sampling estimator based on many Gaussians with time-varying properties. At  $t = 1$ , the Gaussians are wide and overlapping and near  $t = 0$  they approach delta peaks. If the number of samples drawn for each importance sampling distribution is  $N_i = 1, \forall i$ , then the estimator  $\hat{p}_t$ , simplifies to

$$\hat{p}_t(\mathbf{x}) = \sum_{i=1}^{N_{\text{ens}}} \kappa_t(\mathbf{x}|\mathbf{x}'_i) \frac{p_0(\mathbf{x}'_i)}{\sum_{j=1}^{N_{\text{ens}}} \kappa_t(\mathbf{x}'_i|\mathbf{x}_j)}, \quad \mathbf{x}'_i \sim \kappa_t(\cdot|\mathbf{x}_i), \tag{21}$$

which resembles an importance sampling estimator where the importance sampling distribution is a mixture of Gaussians with equal weights. We found that this estimator can be favorable over the simple Gaussian one presented in the main text for problems that are highly non-Gaussian, e.g., the “banana” distribution in Figure 9.

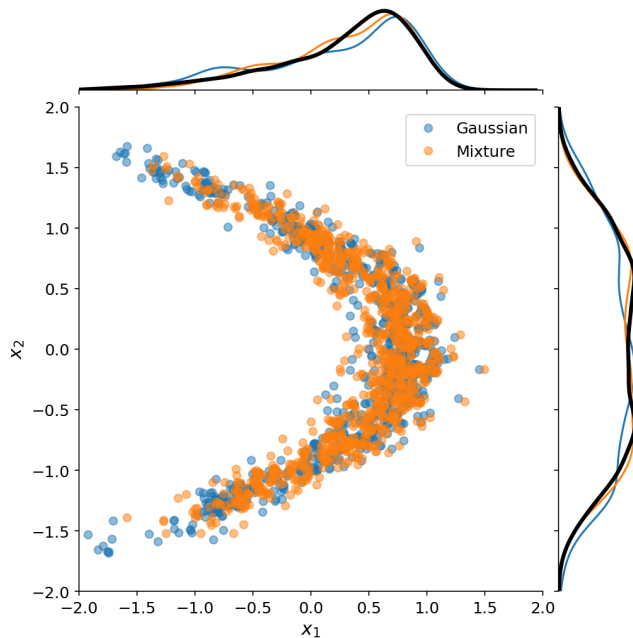


Figure 9. Comparison of samples from the “banana” distribution using either the **Gaussian importance sampling** distribution (blue) or the **multiple importance sampling** distribution corresponding to a mixture of Gaussians (orange). The black line in the marginal plots indicates the ground truth probability density. While both importance sampling distributions result in accurate samples from the “banana” distribution, the mixture distribution leads to probability densities that are slightly closer to the ground truth.